ACSNANO

www.acsnano.org

ARTICLE

Active Antifogging Property of Monolayer SiO_2 Film with Bioinspired Multiscale Hierarchical Pagoda Structures

Zhiwu Han,[†] Zhengzhi Mu,[†] Bo Li, Ze Wang, Junqiu Zhang, Shichao Niu,[*] and Luquan Ren

Key Laboratory of Bionic Engineering, Ministry of Education, Jilin University, Changchun 130022, People's Republic of China

Supporting Information

ABSTRACT: Antifogging surfaces with hydrophilic or even superhydrophilic wetting behavior have received significant attention due to their ability to reduce light scattering by film-like condensation. However, a major challenge remains in achieving high-speed antifogging performance and revealing the hydrophilic-based antifogging mechanism of glass or other transparent materials under aggressive fogging conditions. Herein, with inspiration from the fog-free property of the typical *Morpho menelaus terrestris* butterfly (Butler, 1866) wing scales, a monolayer SiO_2 film with multiscale hierarchical pagoda structures (MHPSs) based on glass substrate was designed and fabricated using an optimized biotemplate-assisted wet chemical method without any post-treatments. The biomimetic monolayer film (BMF) composed of nanoscale SiO_2 3D networks displayed excellent antifogging properties, which is superior to that of the glass substrate itself. The MHPS-based BMF even kept high transmittance (~95%) under aggressive fog conditions, and it almost instantaneously recovered to a fog-free state (<5 s). Moreover, the underlying active antifogging strategy gathering initial fog capture and final antifog together was revealed. The fogdrops spontaneously adhered on the BMF surface and rapidly spread along the MHPSs in an anisotropic way, which made the fogdrops evaporate instantaneously to attain an initial fog-free state, leading to an efficient active antifogging performance. These properties mainly benefit from the synergistic effect of both hydrophilic chemical compositions (nanoscale SiO_2) and physical structures (biomimetic MHPSs) of the BMF. High-speed active antifogging performance of the glass materials enabled the retention of a high transmittance property even in humid conditions, heralding reliable optical performance in outdoor practical applications, especially in aggressive foggy environments. More importantly, the investigations in this work offer a promising way to handily design and fabricate quasi-textured surfaces with multiscale hierarchical structures that possess high-performance physicochemical properties.

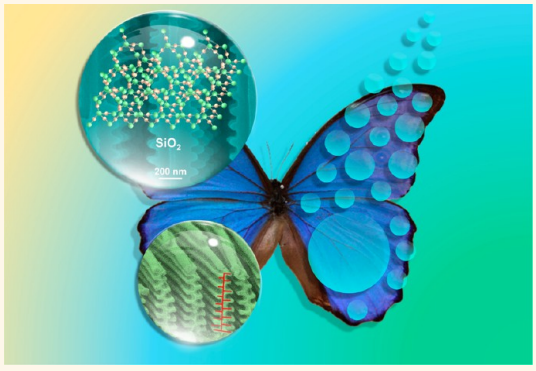

KEYWORDS: *active antifogging property, monolayer SiO_2 film, multiscale hierarchical structures, butterfly wings, biotemplate fabrication*

Fog formation on transparent surfaces is ubiquitous and constitutes a major challenge for optical devices requiring high light transmission, such as eyeglasses, periscopes, goggles, face shields, binoculars, automobile windshields, solar cells, laparoscopes, and medical and analytical instruments.[1−5] Since fogdrops can remarkably reduce the effectiveness of light transmission and therefore optical efficiency, it is a definite concern and considered as a safety hazard and a hindrance both in daily life and technological applications.[6] In this regard, the antifogging property of optical surfaces is pretty significant for developing materials or devices that can be applied and operated in an aggressive foggy environment. In recent decades, researchers have concentrated on improving the antifogging properties of all kinds of designed surfaces. Various methods and techniques have been explored to design and fabricate antifogging coatings (AFCs), such as layer-by-layer assembly,[1,7,8] electrophoretic deposition,[2] covalent grafting,[3] self-masked plasma etching,[4] spin-coating technology,[5] rational synthesis,[9] template-assisted method,[10] and so forth.[6] Despite the AFCs being feasible for preventing fog formation on substrate surfaces and imparting them with antifogging properties, there are some disadvantages in AFCs that need to be overcome, such as the control of coating conditions and adhesive failure caused by thermal mismatch, particularly the poor interfacial adhesion among composite

Received: June 13, 2016
Accepted: July 21, 2016
Published: July 21, 2016

DOI: 10.1021/acsnano.6b03884
ACS Nano 2016, 10, 8591−8602

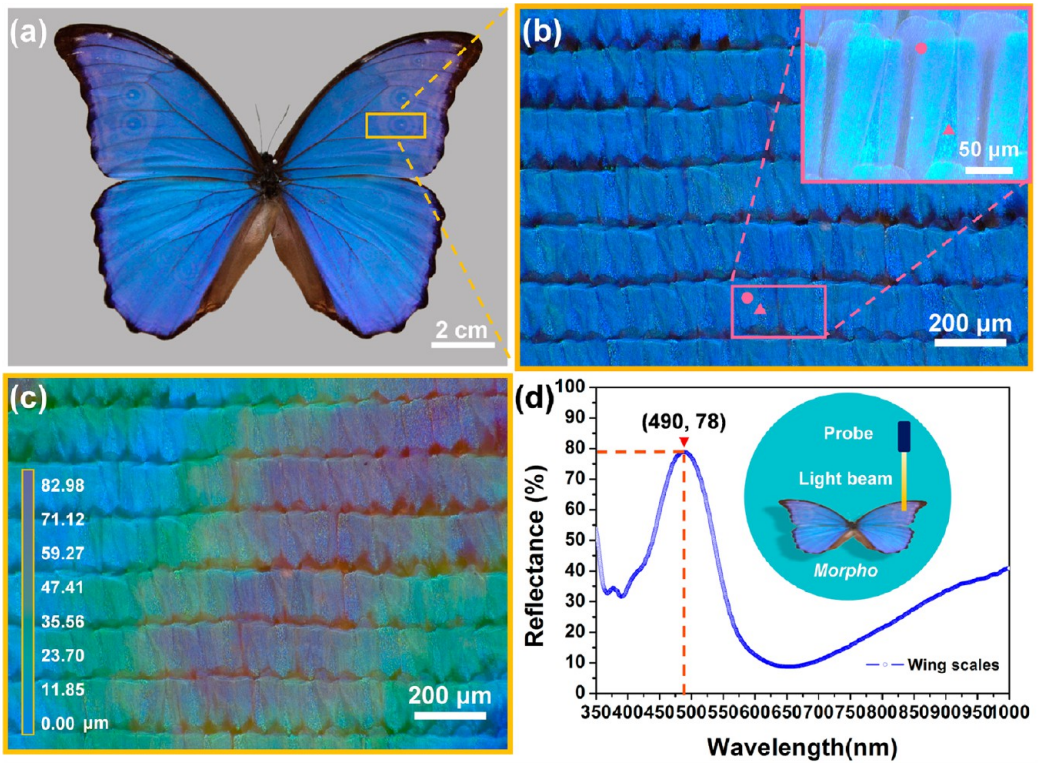

Figure 1. ***Morpho menelaus terrestris*** **butterfly and reflectance spectrum of butterfly wing scales. (a) Digital picture of an individual male butterfly. (b) Stereoscopic microscopy image of the brilliant blue scales demonstrates two types of scales: glass scales and ground scales (inset). (c) Rough wing surface with height distributions ranging from 0 to 82.98 μm. (d) Reflectance spectrum of the wing scales shows a strong peak (78%) at the blue light wave band (490 nm), which is consistent with the result observed by naked eyes.**

multilayers.[3,11] However, antifogging structures (AFSs) can effectively solve the fog formation by controlling and optimizing the interactions between micro-/nanostructures and droplets. Because of the monolithic micro-/nanostructures and homogeneous materials of the AFSs, it exhibits some distinct advantages compared to AFCs, such as long-term mechanical stability, robust durability, and better adherence to the underlying substrate. Therefore, optimal design and controllable fabrication of homogeneous materials with monolithic micro-/nanostructures has become a research hotspot and a significant issue to achieve excellent antifogging properties.

In fact, abundant and gorgeous species in nature give ponderable hints to material scientists and engineers, inspiring them to design and fabricate functional materials and surfaces with morphological structures.[12−16] Some typical fog/water-related natural masterpieces include self-cleaning lotus leaves,[17] cactus with a fog collection system,[18] mosquito compound eyes with dry-style antifogging properties,[19] the peristome surface of *Nepenthes alata* that enables directional water transport,[20] water strider legs with fine nanogrooves,[21] pollen grains with foldable moisturizing structures,[22] and the *Hercules* beetle with a spongy multilayer.[23] In particular, there has been increasing interest in butterfly wing scales due to their ultrafine multiscale hierarchical micro-/nanostructures, which is becoming a research hotspot in the bionics field.[24,25] To date, vast discoveries on butterfly wings have shown that some functional micro-/nanostructures in wing scales actually possess advantageous physicochemical properties and have potential values in wide application prospects, such as selective gas sensors,[26] effective solar collectors,[27,28] tunable optical filters,[29] multiple antireflective surfaces,[30] and so on.[31−33] Remarkably, the fog-free property of butterfly wing scales has not received much attention, and the antifogging mechanism of multiscale hierarchical pagoda structures (MHPSs) in butterfly wing scales is not clear and unified so far. In addition, most existing antifogging surfaces were employed in relative passive strategies to restrain fog formation, namely, only when more and more fogdrops condense on the surfaces to form a big water drop can the passive antifogging strategies work. Unfortunately, these passive strategies remarkably increased the antifogging time up to minutes or even longer and reduced the antifogging efficiency to some degree. However, *Morpho menelaus terrestris* butterfly, a typical butterfly living in tropical rainforests, can handle this puzzle smartly and efficiently *via* MHPSs, a kind of AFS, in its wing scales.

Inspired by this, herein, we investigated the fog-free properties of butterfly wing scales. Then, a SiO_2 biomimetic monolayer film (BMF) was fabricated successfully *via* a simple and effective sol−gel method and selective etching process. The MHPS-inspired active antifogging property of this film was characterized in detail. Interestingly, BMF dramatically demonstrates a superhydrophilic property and is able to rapidly capture surrounding fogdrops then regulates their behaviors on its textured surface. Furthermore, the underlying active antifogging mechanism gathering fog capture and anisotropic spread together was fully revealed. It was surprisingly discovered that the MHPS-based BMF can even keep high transmittance (~95%) under aggressive foggy conditions and almost instantaneously recover to a fog-free state (<5 s).

DOI: 10.1021/acsnano.6b03884
ACS Nano 2016, 10, 8591−8602

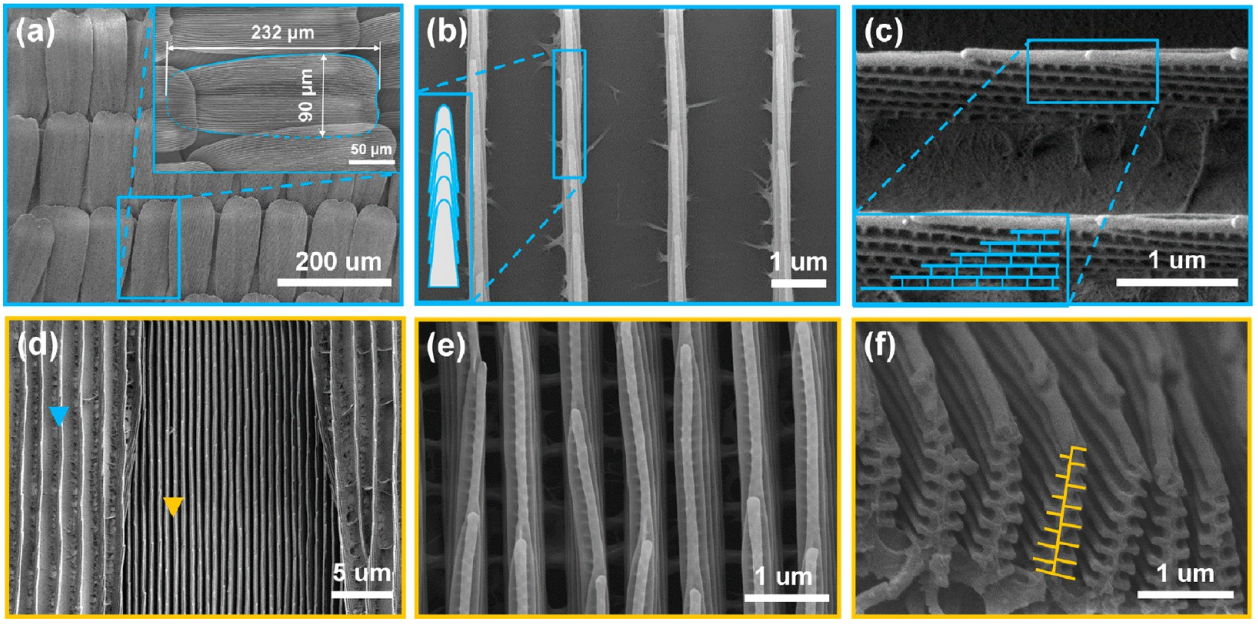

Figure 2. FESEM images demonstrate the feature structures of the original cover scales (a–c) and ground scales (d–f). (a) Shapes and distributions of the original scales on the butterfly wing substrate. A single scale (inset) shows its feature sizes in length and width. (b) Periodic parallel ridges arrange along the length of the wing scales. The overlapped lamellae (inset) constitute these narrow ridges. (c) Side view of the ridges shows the ultrafine window-like structures (inset) between two adjacent lamellae. (d) Overlapping region of cover scales (blue triangle) and ground scales (yellow triangle). (e) Denser ridges with similar multiscale hierarchical structures. (f) Cross section of the ridges demonstrates typical pagoda structures (yellow profile).

RESULTS AND DISCUSSION

Biological Prototype and Its Wing Scales under Macroscopic and Micro-/Nanoscale Levels. In this work, *Morpho menelaus terrestris* butterfly, a subspecies of *Morpho menelaus*, was selected as the biological prototype for its typical foggy and humid habitat.[34] In fact, it is distributed across a wide range of tropical rainforests in the world, especially Central America and South America, and is famous for its huge individual and brilliant blue color. The wingspan of a male *Morpho menelaus terrestris* butterfly is approximately 14 cm (Figure 1a), and the dorsal wings consist of overlapping microscales with mysterious uniform blue brilliance. With the help of ultradepth 3D stereoscopic microscopy, the brilliant blue scales lined up and the micromorphologies of the wing scales were observed (Figure 1b). Interestingly, the wing scales were distinctly divided into two types: transparent cover scales (CSs) and blue ground scales (GSs), as marked by the pink rectangle. They worked together to be responsible for the brilliant physical colors.[35−37] Height distributions of the wing scales in the vertical direction to the wing surface were obtained (Figure 1c). It was indicated that the wing surface is virtually rough rather than seemingly smooth. On one hand, the maximal height difference reaches 82.98 μm, which enhanced the wing surface roughness on a macroscale. On the other hand, a simple discoloration experiment was carried out to confirm that the macroscopic physical colors arise from the micro-/nanostructures in wing scales. These structures further increased the wing surface roughness at the micro-/nanoscale level. It can be seen that the colors changed from blue to green and then recovered to blue when the specimen dried naturally. The blue color was still brilliant, which was not affected by the organic solvents (Figure S1). The results of the discoloration experiment (Video S1) provided an assisted proof that the micro-/nanostructures did exist in the original wing scales. Furthermore, the optical properties of the rough wing surface were carefully determined using a miniature fiber-optic spectrometer with a metal probe. The corresponding reflectance spectrum over a range of 350−1000 nm wavelengths was obtained at normal incidence. A strong reflectance peak appeared at 490 nm, and the maximal reflectance value was approximately 80% in the visible region, which was exactly consistent with the blue color (Figure 1d). In fact, butterfly wing scales are effective and functional units for special physicochemical properties. The ingenious overall configurations and micro-/nanostructures of these wing scales are also the crucial factors for function design and biomimetic fabrication in this work.

Morphology Characterizations, Composition Analysis, and Wettability of the Rough Wing Surface with MHPSs. As characterized by field emission scanning electron microscopy (FESEM), the multiscale hierarchical morphologies of the original wing scales were observed in detail under different magnifications (Figure 2a–f). A close-up view showed these overlapping tiny scales with oval shapes like tiles on the roof with sizes of 90 μm wide and 232 μm long (Figure 2a). The scale density varies from 50 to 60 scales per square millimeter. The intensive wing scales run approximately parallel to the scale substrate and fall into two types (CSs and GSs) in an alternated manner. CSs are on the superstratum, and GSs are on the substratum (Figure 2d). CSs and GSs overlap each other, and both of them possess ridge-trench complex arrays with different periodic spacing. Specifically, the spacing between two adjacent ridges of CSs is about 2 μm (Figure 2b), which is much broader than that of GSs (Figure 2e). In addition, the ridge width of CSs is about 200 nm, whereas that of GSs is much broader (~400 nm). Every ridge consists of several layers of lamellae paralleled to each other (Figure 2c). There exist numerous even-distributed microribs that form

DOI: 10.1021/acsnano.6b03884
ACS Nano 2016, 10, 8591−8602

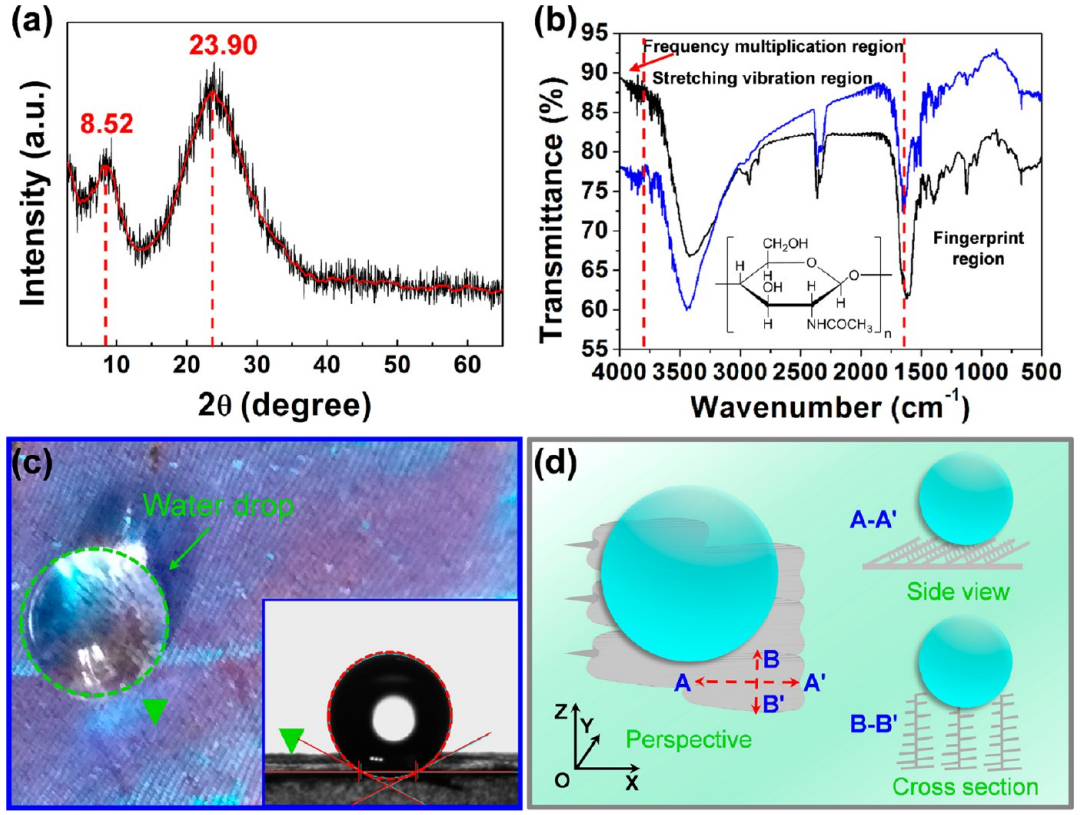

Figure 3. (a) XRD spectrum of MHPS presents its quasi-PC structures and corresponding grazing angles. (b) Fourier transform infrared spectra of original (black line) and treated (blue line) wing scales for comparison indicate the brilliant blue colors result from fine micro-/nanostructures in wing scales rather than pigments. (c) Digital photo and CA measurement image (inset) of the wing surface (green triangle) show excellent superhydrophobic property. (d) Simplified illustrations of the static behaviors of a single water drop on a butterfly wing from two different views.

rows of window-like pits between two adjacent lamellae. In order to obtain 3D morphologies of the ridges, original wing scales were crosscut by a scalpel along a direction perpendicular to the ridges. Then, the cross section of the ridges was observed (Figure 2f). Interestingly, the cross section of a single ridge shows a typical "pagoda" shape. In general, both CSs and GSs are of the similar multiscale hierarchical structures, including ridges, lamellae, and ribs. Herein, we called the complex structures MHPSs. More FESEM images depicting the 3D fine MHPSs under other view angles are available (Figure S2). In fact, the MHPS can be regarded as a kind of photonic crystal (PC).[36] As characterized by X-ray diffraction (XRD), the crystal structure characteristics of MHPSs were obtained (Figure 3a). Based on Bragg's law, the relationship among interplanar spacing (d), grazing angle (θ), and X-ray wavelength (λ) can be quantitatively described eq 1 as follows:

$$2d \sin \theta = n\lambda \quad (1)$$

where n is diffraction series that could be any positive integer. In the XRD spectrum, two strong Bragg peaks appear at 4.26 and 11.95°, which further confirms the periodic character of the MHPSs in original wing scales.

When it comes to the chemical compositions, just as other insects in nature,[38] the original wing scales in the *Morpho* butterfly are mainly chitin-based[39−41] and primarily composed of water-insoluble organic components. The major elements include carbon (C), hydrogen (H), oxygen (O), and nitrogen (N), which constitute the nonwetting organic framework of MHPSs. According to Fourier transform infrared (FTIR) spectra, the characteristic peaks of processed wing scales are similar to that of original wing scales (Figure 3b). The enhanced absorption peaks of the sample at 667 and 2358 cm^{-1} appeared after the treatment of the original sample by diethyl ether (A.R.) and absolute ethanol (A.R.) for 10 min, respectively, which are attributed to the bending vibration and asymmetric stretching vibration of CO_2. The broad absorption peaks at 3428 and 3260 cm^{-1} correspond to the stretching vibration of hydroxyl groups (−OH) and the N−H bond. The weak absorption peaks at 2966, 2923, and 2874 cm^{-1} are assigned to the stretching vibration of the C−H bond. The multipeaks at 1655, 1550, and 1310 cm^{-1} around the fingerprint region are assigned to amide I, amide II, and amide III, which are the characteristic groups of chitin. The weak peak around 1076 cm^{-1} is assigned to the stretching vibration of the C−O bond, and the very weak peak around 886 cm^{-1} is assigned to the stretching vibration of the hexatomic ring, which is the backbone of chitin. The results of XRD and FTIR spectroscopy indicated that the pretreatment of the original wing scales hardly changed their chemical compositions and the MHPSs in original wing scales were well-preserved, which provided a foundation for the following function design and biomimetic fabrication of the MHPSs. It is an acceptable principle that the roughness effect can amplify the intrinsic wettability of the substrate surface.[42] Thanks to the merits of the roughness effect due to the MHPSs of wing scales and nonwetting chemical compositions, the wing surface shows excellent superhydrophobic property with a static contact angle (CA) of 155.5° (Figure 3c). Considering butterfly wings'

DOI: 10.1021/acsnano.6b03884
ACS Nano 2016, 10, 8591−8602

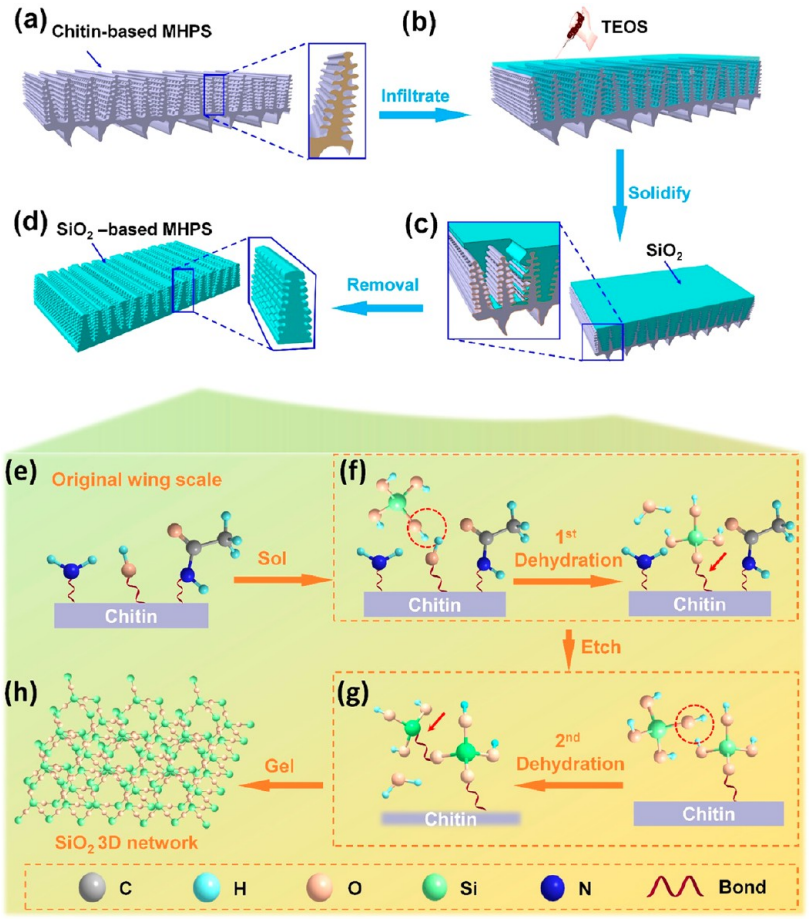

Figure 4. Biomimetic fabrication process of the MHPS-based BMF and the internal chemical synthesis mechanism of 3D SiO_2 networks in MHPSs. (a) Chitin-based MHPSs in original wing scales. (b) Suitable amount of the precursor solution (10 μL) was added to the edge of the assembly with a micropipette. (c) Assembly was heated at 120 °C for 30 min to finalize the design. (d) After the clips were picked, the biotemplate was removed through the selective etching process in a mixture of concentrated nitric acid and perchloric acid (1:1 in volume) at 130 °C for another 30 min. At last, the whole assembly was washed by ultrasonic oscillation for 15 min with deionized water. (e) Exposed chemical groups ($-NH_2$, $-OH$, and $-NHCOCH_3$) on the chitin-based scale surface after being treated by organic solvents (A.R.). (f) First dehydration reaction occurs between orthosilicic acid (H_4SiO_4) and hydroxyl ($-OH$), leading to the combination of metasilicic acid and chitin substrate. An intermediate of the organic–mineral complex was generated. (g) Second dehydration reaction occurs between H_4SiO_4 and the intermediate, leading to growth of inorganic chains. Meanwhile, the chitin substrate was gradually etched by mixed acids, and the organic frame of the biotemplate would break up. (h) As sol–gel processes continue, SiO_2 3D networks gradually formed and extended along the chitin-based biotemplate.

vibration in reality and an asymmetric ratchet effect of the micro-/nanostructures of wing scales (Figure 3d), the excellent superhydrophobic property is very helpful to the wing surface to drive fogdrops away easily, as shown in previous investigations.[33,43,44] It seems that a superhydrophobic surface may be a bright choice toward antifogging. However, it cannot be neglected that most artificial surfaces in practical applications do not always work in a dynamic state, for example, a vibrating state. Thus, how to achieve a high-performance antifogging surface in static state becomes a significant issue. As we know, a superhydrophilic approach (CA $\leq 10°$) is an effective strategy to achieve static antifogging surfaces.[6] The interfacial wettability is mainly determined by chemical compositions and surface micro-/nanostructures (roughness).[45−47] The Wenzel model and Cassie–Baxter model (Figure S3) indicated that true CA could be higher with an increase of roughness if the surface was originally hydrophobic. Otherwise, it will be lower for an originally hydrophilic surface.[48,49] In terms of the roughness effect of MHPSs in the wing surface, it inspired us to design and implement a MHPS-based biomimetic antifogging surface with hydrophilic materials.

Bioinspired Design and Biomimetic Fabrication of the MHPS-Based BMF. Nanoscale silicon dioxide (SiO_2) is a kind of hydrophilic material and can be obtained easily *via* the hydrolysis–condensation reaction of tetraethylorthosilicate (TEOS) at very low cost and normal temperature. The following work is the biomimetic fabrication process of MHPS-based monolayer SiO_2 film. A simple and effective two-step synthesis approach combining a sol–gel method and selective etching processes was used. It was noteworthy that the original wing scales were directly taken as the biotemplate. According to the feature sizes of the wing scales (Table S1), visual 3D optimized configuration models (Figure S4) imitating the micro-/nanostructures of wing scales were built to illustrate the biomimetic fabrication of the MHPS-based BMF. The fabrication process using a biotemplate from wing scales was illustrated briefly (Figure 4a–d), and the corresponding internal chemical synthesis mechanism was described as follows:

DOI: 10.1021/acsnano.6b03884
ACS Nano 2016, 10, 8591–8602

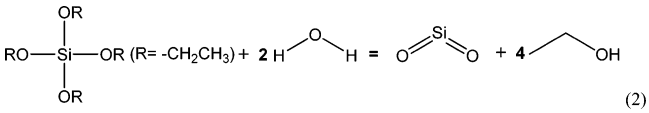

(2)

Herein, TEOS was hydrolyzed to produce hydrated silica and ethyl alcohol at low pH environment. Meanwhile, condensation reactions of TEOS and corresponding hydrated silica occurred to form a colloid mixture, a transparent and homogeneous suspension termed the precursor solution. Then 3D SiO_2 networks making up the biomimetic MHPSs were generated *via* the polymerization reactions of oligomers. In fact, the hydrolysis reaction and condensation reaction together constituted the main body of the aforementioned sol−gel process (Figure 4e−h). The precursor solution filled the lacunas of the MHPSs and became solidified through heat treatment. Solid biomimetic MHPSs were obtained and further formed the expected BMF after the original biotemplate materials were etched away by mixed acids under high temperature (130 °C).

Morphology Characterizations and Composition Analysis of the Biomimetic MHPSs. In order to confirm that the MHPSs in original wing scales were inherited by the BMF, the morphologies and micro-/nanostructures were characterized using FESEM. The BMF consists of numerous chemical self-assembled ridges aligning in an array on the glass substrate. The typical "ridge-gorge" morphology of the BMF surface was illustrated by atomic force microscopy (AFM) (see inset of Figure 5a). Every single ridge was similar to a bramble with thorns from the top view (Figure 5b). The feature sizes of the biomimetic ridges were measured (Figure 5c). The width of single ridge is about 451 nm. The distance between two adjacent ridges is about 783 nm. The radius of papilla-like structures on both sides of the lamellae is about 41 nm. These ridges composed of parallel bramble-like lamellae in sequential horizontal layers from the side view (Figure 5d). It is clear that the cross section of single ridge resembles a typical pagoda structure. Every pagoda-like ridge is a set of micro-multilayer systems with 5−8 alternant SiO_2 and air layers in the vertical direction. The multiscale hierarchical interdependent components including pagoda-like ridges, bramble-like lamellae, and papilla-like structures, worked together to generate the overall MHPS system (Table S2). To compare the surface wettability, the static CA of a glass substrate and BMF was obtained (Figure 6a). Intuitively, the surface wettability of BMF is much better than that of the glass substrate, which was further confirmed by the measurement results of static CA (Figure 6b). The BMF based on the glass substrate was confirmed as a superhydrophilic surface with the static CA value of 6.2°. Besides, their average static CA values are 7.0 and 38.3°, respectively, in three measurements, which further indicated that the roughness of BMF dramatically increased to endow the glass substrate excellent wettability. FTIR spectra of the original wing scales and BMF (Figure S5) were obtained for comparison, which indicated that the chemical compositions of BMF had changed significantly. Furthermore, it confirmed that the original wing scales were decomposed, and the

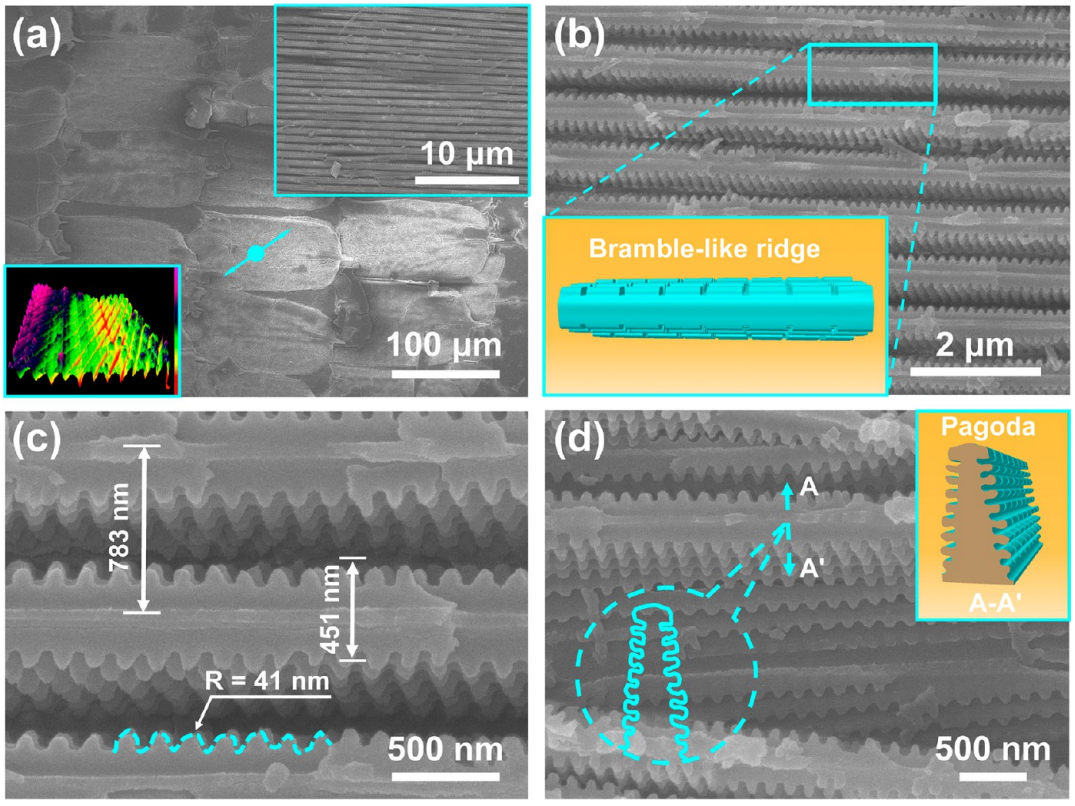

Figure 5. FESEM images of the fabricated MHPS-based BMF under different magnifications. (a) Low-magnification FESEM images and AFM image (color inset) demonstrate overall morphology of the MHPS-based BMF. (b) Enlarged FESEM image demonstrates microstructures of the biomimetic MHPSs, especially the bramble-like ridge (inset). (c) High-magnification FESEM image demonstrates the nanostructures' feature sizes of the biomimetic MHPSs, including ridge and papilla. (d) FESEM image of the biomimetic pagoda structure (inset) from the side view under high magnification.

DOI: 10.1021/acsnano.6b03884
ACS Nano 2016, 10, 8591−8602

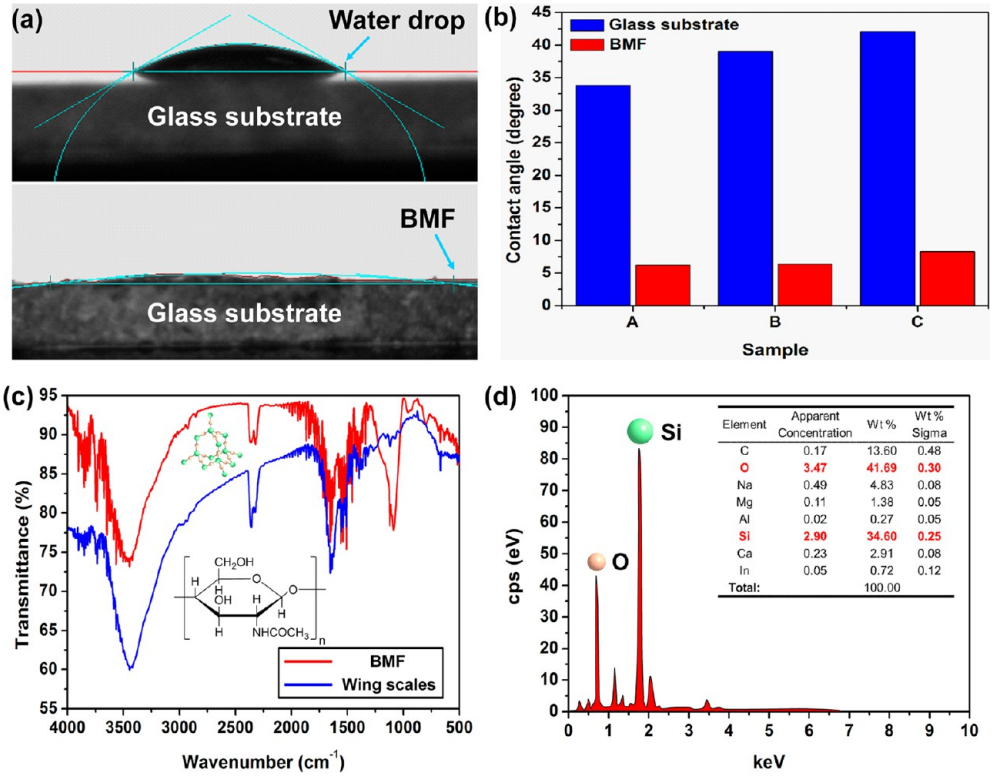

Figure 6. (a,b) Water wettability of the glass substrate and BMF for comparison. (c) FTIR spectra of chitin-based wing scales and SiO_2-based BMF for comparison. (d) EDS spectrum indicates that the main elements of BMF are Si and O, which further proved that the nanoscale SiO_2 was obtained successfully.

expected SiO_2 was achieved *via* a sol−gel process (Figure 6c). Energy-dispersive spectroscopy (EDS) results indicated that the fabricated BMF is mainly composed of two elements, silicon (Si) and oxygen (O), that reach up to 34.60 and 41.69 wt % (Figure 6d and Table S3). It further confirmed that nanoscale SiO_2 was obtained *via* the hydrolysis−condensation reaction of TEOS. In brief, on one hand, hydrophilic nanoscale SiO_2 lays the foundation for the achievement of the superhydrophilic BMF chemically. On the other hand, the biomimetic MHPS system further amplifies the hydrophilic effect (CA = 38.3°) to realize the superhydrophilic effect (CA = 7.0°) physically, which plays a crucial role in the achievement of the active antifogging property. It is chemical compositions (nanoscale SiO_2) and physical structures (biomimetic MHPSs) that work together to achieve the superhydrophilic BMF successfully.

Antifogging Performance of the MHPS-Based BMF. The antifogging property of the BMF was characterized by a self-built spray simulation system (Figure 7a). First, the BMF based on a glass substrate that was fixed by a clip was adjusted to be perpendicular to the light beam. Then, the transmittance spectra changes of the glass substrate (reference substance) and BMF were obtained over a range of wavelengths from 350 to 1000 nm (Figure 7b,c). It can be seen that the glass substrate and BMF were of low transmittance in the short wave band (350−480 nm). The transmittance of BMF (~58%) is much lower than that of the glass substrate (~82%) in its initial state. On one hand, the inherent UV (350−400 nm) absorption property of the glass substrate inevitably reduces the transmittance. On the other hand, the transmittance of blue light (400−480 nm) would decrease due to the integrated effect of reflection and refraction that occurred in part of the MHPS in the BMF. It is consistent with the blue structural color of the BMF. However, the maximal transmittance of BMF (~95%) is even better than that of glass substrate (~90%) over a broad wavelength range of 480−1000 nm. It was indicated that the BMF dramatically enhances the transmittance (~5%) of the glass substrate, which confirmed that the BMF possesses excellent visible and infrared anti-reflection properties.

The steady continuous fog was generated and controlled by an ultrasonic humidifier at a constant flow rate of 0.5 mL·min^{-1}. First, the generated fog was sequentially sprayed on the BMF at different times, and the spray time gradually increased within 60 s at an interval of 10 s (Figure 7d). The BMF was blow-dried after the transmittance spectrum was obtained each time, which eventually formed a dynamic cyclical process of "spray−blow−dry−spray". The transmittance in the short wave band (350−480 nm) increased to 84% after the BMF was sequentially sprayed by the generated fog for the first 10 s and eventually decreased to 27%. Interestingly, the maximal transmittances of BMF with respect to different spray times almost remain stable around 95% over a range of wavelengths from 480 to 1000 nm. It was confirmed that the BMF demonstrates high antifogging performance over a broad wavelength range. Furthermore, in order to characterize the antifogging recovery property, the variation trends of the transmittance spectra of BMF were obtained after being sprayed by the generated fog for 60 s (Figure 7e). Likewise, the BMF is of low transmittance (~15%) in the short wave band (350−480 nm) and stable at high transmittance (~95%) over major visible wavelengths (480−780 nm) and near-infrared wavelengths (780−1000 nm). It can be seen that the transmittance spectra have a similar variation trend with the 60 s gradient spray over the whole wavelength (350−1000 nm). However, the transmittance rapidly increased with the recovery time increasing and eventually recovered to

DOI: 10.1021/acsnano.6b03884
ACS Nano 2016, 10, 8591−8602

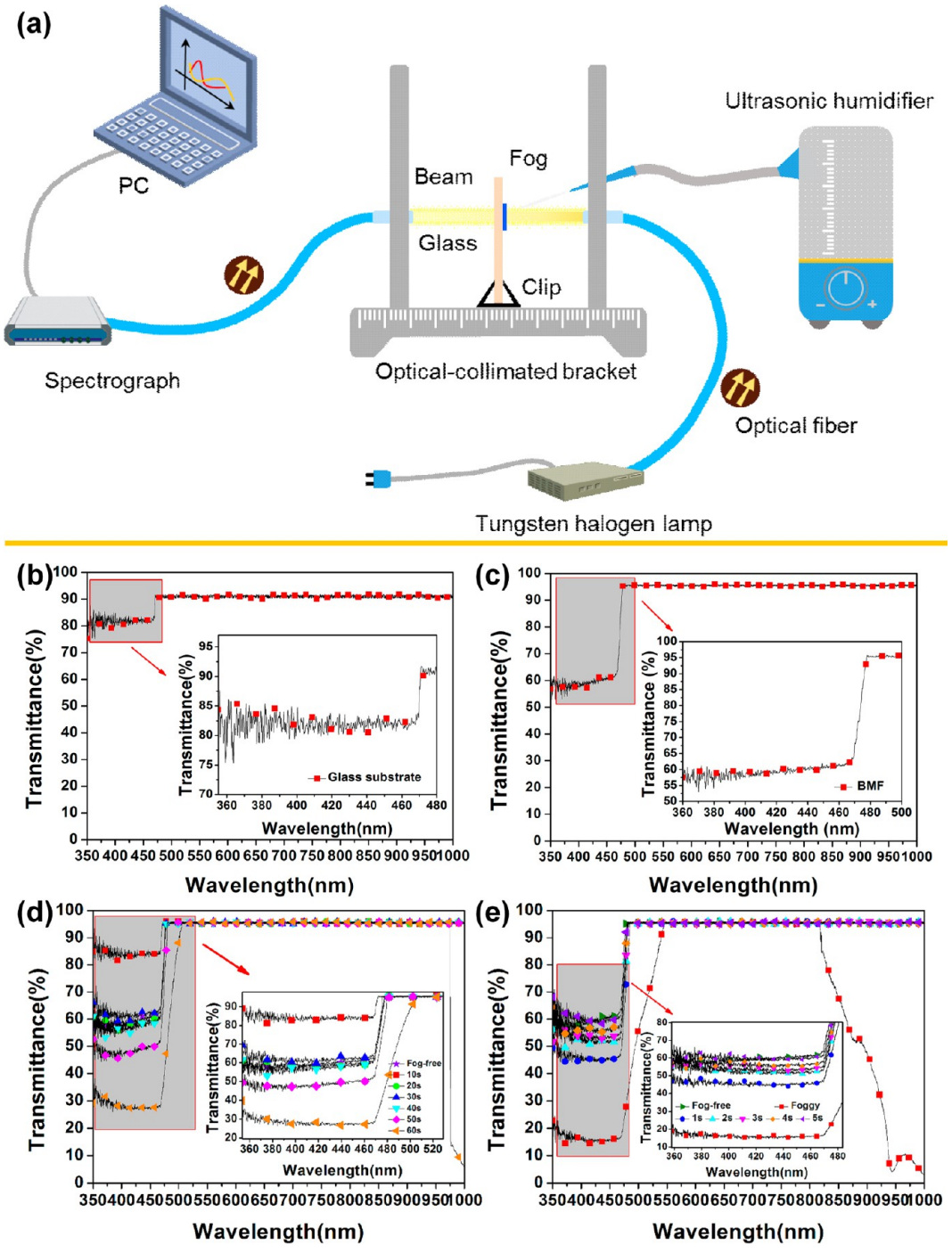

Figure 7. Core components of the self-built spray simulation system and transmittance spectra of the glass substrate and MHPS-based BMF. (a) Schematics of the self-built spray simulation system. (b,c) Initial transmittance spectra of fog-free glass substrate and BMF before spray simulation. (d) Transmittance of the BMF changes at intervals of 10 s during gradient spray simulation for 60 s. (e) Transmittance recovers to initial fog-free state after continuous spray simulation for 60 s.

the initial fog-free state (~58%), which is especially obvious in the short wave band (350−480 nm). It was confirmed that the MHPS-based BMF possesses superior antifogging recovery property (~5 s), which is conducive for its reutilization.

Active Antifogging Mechanism of the BMF with MHPSs. For a more detailed analysis of the antifogging behaviors of the BMF, the dynamic behaviors of the drippy fogdrops on the surface of BMF were intuitively observed using a high-speed camera system (Video S2). It can be seen that the BMF is in a foggy atmosphere at the beginning. Then, the floating water vapor condensed rapidly into fogdrops on the BMF, which gradually grew to be visible and bright. Subsequently, the foggy atmosphere disappeared rapidly within a matter of seconds. Meanwhile, the BMF recovered to its initial transparent state without fogdrops. The observations are exactly consistent with the corresponding transmittance spectra of the BMF.

To illustrate the antifogging behaviors of the BMF, simplified 3D MHPS models of the original wing scales and the BMF were built up, which was based on their FESEM observations.

DOI: 10.1021/acsnano.6b03884
ACS Nano 2016, 10, 8591−8602

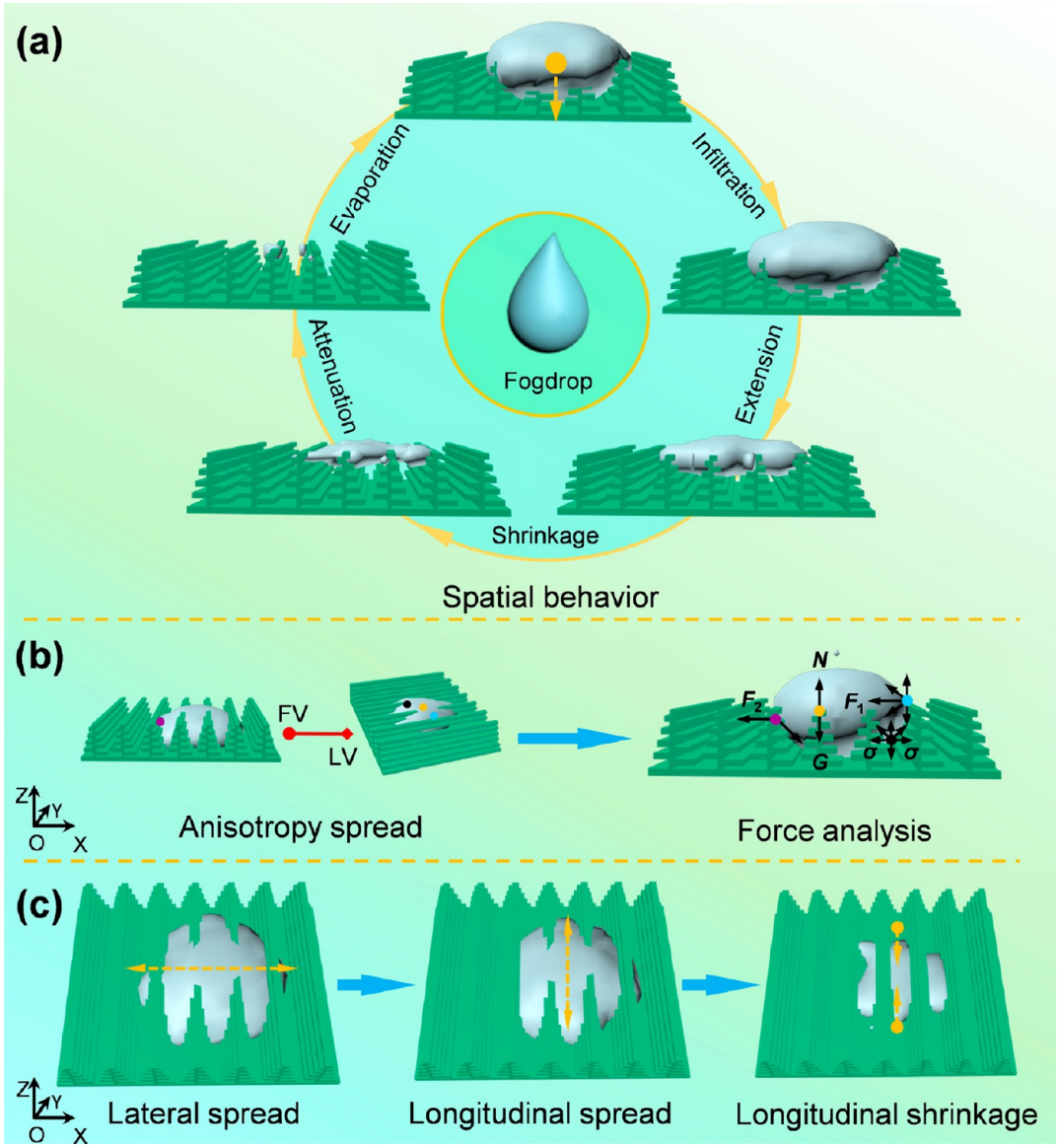

Figure 8. Active antifogging behaviors of the MHPS-based BMF. (a) Spatial behaviors of the fogdrop on the BMF surface. (b) Static microforce analysis of the fogdrop. Here, FV and LV represent front view and lateral view, respectively; *N* is normal force, *G* is gravity, F_1 is intermolecular force, F_2 is attractive force, and σ is surface tension. (c) Anisotropic spread of a fogdrop on the MHPS-based BMF surface.

According to the results of transmittance spectra measurements and high-speed video observations, the whole active antifogging behaviors of the BMF were illustrated annularly (Figure 8a) and artificially divided into two steps for illustrative purposes (Figure S6). Herein, step one was the so-called "fogdrop capture". The surroundings of the MHPSs in BMF could be suffused with tiny drops of water that were derived from the generated fog. Then, the fogdrops that contacted the surface of MHPSs spontaneously adhered to form a hydrone monolayer. The adhering layer in the interface region attracted an adjacent water cluster that was composed of some hydrones to wet the MHPSs. Meanwhile, the fogdrops would gradually grow with more and more water clusters aggregating by hydrogen bonds. Step two was the so-called "anisotropic spread" (Figure 8b). The grown fogdrop spread spatially along the *x*-axis, *y*-axis, and *z*-axis at different rates due to the unbalanced forces. Apparently, the spread rate along the *y*-axis was faster than that along *x*-axis, and the spread rate along *z*-axis was the slowest (Video S3). The fundamental cause of the anisotropic spread lay in the MHPSs that formed narrow layered passageways. The fogdrop along the *y*-axis spread rapidly through every passageway without any obstacles, whereas that along the *x*-axis spread slowly due to the physical obstruction of the MHPSs. Because of the combined effect of both gravity and surface tension, the fogdrop along the *z*-axis spread the slowest. Soon the whole fogdrop would be split in several tiny drops with different sizes by the raised ridges of the MHPSs. It was amazing to note that the large specific surface areas of the MHPSs play an important role in promoting the rapid evaporation of these tiny drops. Eventually, the fogdrops disappeared completely, and the BMF recovered to the initial high transmittance state. All of these processes formed an active antifogging cycle of "fogdrop capture−anisotropic spread−rapid evaporation".

In order to further reveal the internal active antifogging mechanism of the BMF, one possible reasonable explanation for these findings was that the synergistic effect of both chemical compositions and physical structures of the BMF was

DOI: 10.1021/acsnano.6b03884
ACS Nano 2016, 10, 8591−8602

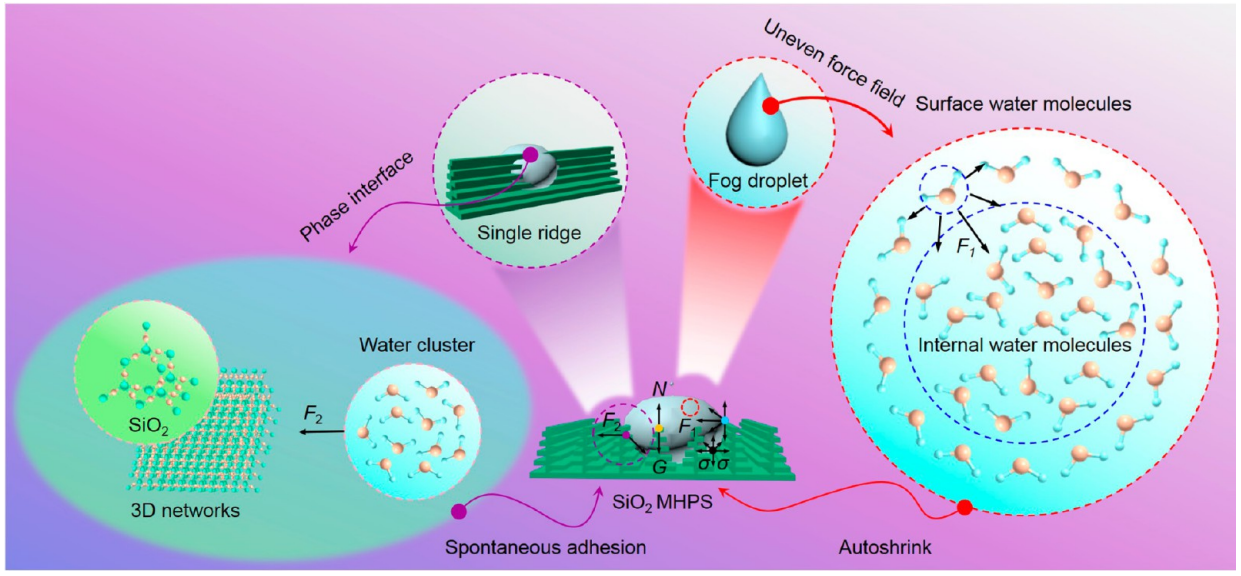

Figure 9. Synergistic effect of chemical compositions and MHPSs of the BMF, realizing the active antifogging property.

the key factor to realize the active antifogging property (Figure 9). On one hand, the hydrophilic hydroxyls (−OH) that joined with Si atoms of the BMF composed of SiO_2 3D networks had strong adsorption ability for hydrones in air, which was chemically conducive for capturing fogdrops around the BMF. This could increase the surface hydrophilicity with the increase of the hydrones and lead to the spontaneous adhesion. Physically, the fogdrops would keep close to the MHPSs and then shrink directionally due to the uneven force field. On the other hand, it is a universal strategy to construct the superhydrophilic surface by creating rough structures with hydrophilic components. Interestingly, the MHPSs of the BMF played a significant role in amplifying the intrinsic wettability of the glass substrate, which dramatically increased the surface roughness. In fact, the relationships between CA and roughness ratio in two different wettability states were quantitatively described as the Wenzel model and Cassie−Baxter model, which indicated that the true CA of original hydrophilic surface would be lower with the increase of surface roughness. Apparently, it was the hierarchical amplification effect of MHPSs that brought big rewards for the achievement of the superhydrophilic surface. In addition, with the increase of the hydrophilic specific surface that arose from the fabricated MHPSs, the surface free energy was obviously enhanced. According to the lowest energy principle, hydrones preferred to stay in the nanoscale structures of the BMF to achieve a minimum energy state, which may induce the transition of the fogdrops from a metastable Cassie−Baxter impregnating wetting state to a stable Wenzel state. Due to the active capture and anisotropic spread of the grown fogdrops, the MHPSs rapidly got wet and the BMF was soon covered with a thin water film. Then the refraction of incident light would occur at the interface between air and the thin water film. Typically, short waves including the UV and blue−violet light were refracted strongly, and the transmittances of that significantly decreased. However, the thin water film would evaporate rapidly due to the increase of the effective contact area between fogdrops and the MHPSs with large specific surface. Consequently, the transmittance of the BMF would recover to the initial state. These were exactly consistent with the results of transmittance spectra.

CONCLUSION

In summary, it was confirmed that the structure-based colorful surface of the *Morpho menelaus terrestris* butterfly wing endows itself excellent fog-free properties. The SiO_2 MHPS-based BMF was successfully fabricated *via* a simple and effective biomimetic fabrication method combining a sol−gel process and subsequent selective etching. Then, the high-speed antifogging properties of the MHPS-based BMF were characterized experimentally using a self-built spray simulation system. The BMF was composed of nanoscale 3D SiO_2 networks and displayed excellent antifogging properties, which is superior to that of the glass substrate. The MHPS-based BMF can even keep high transmittance (~95%) under aggressive foggy conditions (ν_{spray} = 0.5 mL·min^{-1}) for 60 s, and it could recover to a fog-free state within 5 s. According to the observation results, the dimensions and distributions of MHPSs in the BMF were achieved. Meanwhile, a set of visual 3D-optimized models was generated to illustrate the MHPSs and biomimetic fabrication process. Moreover, the underlying active strategy combining initial fog capture and final antifogging behaviors was revealed. The fogdrops spontaneously adhered on the BMF surface and rapidly spread along the MHPSs in an anisotropic way, which made the fogdrops evaporate instantaneously to attain an initial fog-free state, leading to an interesting active antifogging performance. The findings of this work offer a facile and effective strategy for fabricating antifogging surfaces and suggest great potential value for particular antifogging applications, such as car windows, glass curtain walls, high-precision lenses, endoscopes, and so forth. Therefore, we anticipate that the MHPSs of the butterfly wing scales with excellent physicochemical properties may inspire more scientists and engineers to focus on mimicking natural structures in a simple and effective route and to design more ingenious engineering products with desirable functionalities in the future.

EXPERIMENTAL SECTION

Biological Prototype. The wing scales of male *Morpho menelaus terrestris* butterflies were used as experimental materials in this work.

Discoloration Experiment. First, a neat and clean wing patch was meticulously cut off the fore wings with a scalpel in perpendicular and

DOI: 10.1021/acsnano.6b03884
ACS Nano 2016, 10, 8591−8602

parallel directions to the nervure. Then, the specimen was placed flatwise in a culture dish with a cuspidal tweezer and soaked in a certain amount of diethyl ether and absolute ethanol for 10 min, which increases the mechanical strength of the wing patch. Subsequently, the specimen was taken out and its color changes were observed with the naked eye. Diethyl ether and absolute ethanol were provided by Sinopharm Chemical Reagent Co., Ltd. All reagents were of analytical grade (A.R.) without further purification.

Fabrication Process of the SiO_2 MHPS-Based BMF. The SiO_2 BMF was fabricated using a facile wet chemical biomimetic fabrication method combining a sol−gel process and selective etching. First, slices of the pretreated wings (1 cm × 2 cm) were sandwiched between two clean glass slides, of which both ends were clamped by clips with proper force. The precursor solution with a volume of 10 μL, a compound of TEOS and hydrochloric acid (3:1 in volume), was added to the edge of the assembly by a micropipet. Due to the capillary action between the glass slides, the precursor solution infiltrated the microstructures of the wing scales spontaneously. The entire assembly was heated at 120 °C for 30 min in a drying oven to evaporate residual solvent, and the precursor solution in the microstructures of the wing scales further solidified to form the SiO_2 MHPSs. Then, the clips were picked down with a tweezer carefully to avoid destroying the crisp microstructures. After that, the whole assembly was dipped into a mixture of concentrated nitric acid and perchloric acid (1:1 in volume) while being heated at 130 °C for another 30 min. The biotemplate was removed due to the corrosive effect of the mixed acids. At last, the whole assembly was washed by ultrasonic oscillation for 15 min with deionized water. Finally, the BMF with SiO_2 MHPSs based on a glass substrate was reserved in slots of a slide box. Concentrated nitric acid (A.R.) and TEOS were provided by Beijing Chemical Works, and perchloric acid and hydrochloric acid were provided by Changchun Hongyu Chemical Co., Ltd.

3D Stereoscopic Microscopy. With the help of ultradeep 3D stereoscopic microscopy (KEYENCE VHX-5000), the morphologies and dimensions of original wing scales were characterized under different magnifications.

Scanning Electron Microscopy. The original wing scales and BMF based on a glass substrate were dried in air at room temperature and visualized by SEM (ZEISS EVO18) using an accelerating voltage of 10 kV and working distance of 10 mm.

X-ray Diffraction. An XRD sample was fixed on the sample stage to keep it even. The quasi-PC structures were characterized using an X-ray diffractometer (Rigaku). The experiment data were collected from 3 to 65°.

Atomic Force Microscopy. AFM samples were prepared similarly to the SEM samples. Samples were placed on the mica plates. Images were obtained using AFM (Bruker's Dimension Icon ScanAsyst) with cantilevers/tips and analyzed by the software NanoScope Analysis.

Fourier Transform Infrared Spectroscopy. In order to achieve the FTIR spectra of the original wing and the activated wing using a FTIR (Bruker EQUINOX 55) instrument, the samples were mashed to powder and compressed into KBr (A.R.) pellets.

Energy-Dispersive Spectroscopy. The compositions and distributions of the main elements in the SiO_2 BMF were measured using EDS (OXFORD X-Max^N 150).

Static Contact Angle Measurements. The static water contact angles of the original wings and the fabricated SiO_2 BMF were estimated with a contact angle meter (JC2000A Powereach, China) based on a sessile drop measuring method with a water drop volume of 3 μL.

Spray Simulation. The self-built spray simulation system includes a tungsten−halogen lamp (Ocean Optics LS-1-LL), optical fiber, ultrasonic humidifier (YADU YC-X100E), optical-collimated bracket, a spectrograph (Ocean Optics USB 4000), and a laptop computer.

Dynamic Observation of Fogdrop Behaviors. The dynamic observation using a high-speed camera (PCOdimax HD) was carried out. In this work, the macrolens was perpendicular to the BMF surface, and the distance between the macrolens and BMF surface was approximately 9 cm.

Reflectance and Transmittance Spectra. The reflectance and transmittance spectra of the BMF were obtained using a miniature fiber-optic spectrometer (Ocean Optics USB 4000), and the light spot size of the incident beam was about 5 mm in diameter. The spectrometer was carefully calibrated with STD-WS, a standard white board certified by the National Institute of Metrology of China.

ASSOCIATED CONTENT

Supporting Information

The Supporting Information is available free of charge on the ACS Publications website at DOI: 10.1021/acsnano.6b03884.

Butterfly wing slice in the discoloration experiment, structural characterizations (FESEM images of pagoda structures from different views), wetting states of solid surfaces to water, structural feature sizes of chitin-based MHPSs in original wing scales and the SiO_2-based MHPSs in BMF, 3D visual models (MHPSs in original butterfly wing scales), structural characterizations of SiO_2-based MHPSs in BMF, chemical composition characterization of SiO_2-based BMF (FTIR and EDS) (PDF)

Video S1: overall colors changing processes in the discoloration experiment (AVI)

Video S2: dynamic behaviors of the drippy fogdrops on the BMF surface (AVI)

Video S3: active antifogging loop and anisotropic spread behaviors (AVI)

AUTHOR INFORMATION

Corresponding Author

*E-mail: niushichao@jlu.edu.cn.

Author Contributions

†Z.H. and Z.M. contributed equally.

Notes

The authors declare no competing financial interest.

ACKNOWLEDGMENTS

This work is supported by the National Natural Science Foundation of China (Nos. 51325501, 51505183, 51290292, and 51175220), and China Postdoctoral Science Foundation Funded Project (No. 2015M571360).

REFERENCES

(1) Xu, L. Q.; He, J. H. Antifogging and Antireflection Coatings Fabricated by Integrating Solid and Mesoporous Silica Nanoparticles without Any Post-Treatments. *ACS Appl. Mater. Interfaces* **2012**, *4*, 3293−3299.

(2) Lai, Y. K.; Tang, Y. X.; Gong, J. J.; Gong, D. G.; Chi, L. F.; Lin, C. Q.; Chen, Z. Transparent Superhydrophobic/Superhydrophilic TiO_2-Based Coatings for Self-Cleaning and Anti-Fogging. *J. Mater. Chem.* **2012**, *22*, 7420−7426.

(3) Chevallier, P.; Turgeon, S.; Sarra-Bournet, C.; Turcotte, R.; Laroche, G. Characterization of Multilayer Anti-fog Coatings. *ACS Appl. Mater. Interfaces* **2011**, *3*, 750−758.

(4) Di Mundo, R.; d'Agostino, R.; Palumbo, F. Long-Lasting Antifog Plasma Modification of Transparent Plastics. *ACS Appl. Mater. Interfaces* **2014**, *6*, 17059−17066.

(5) Park, J. T.; Kim, J. H.; Lee, D. Excellent Anti-Fogging Dye-Sensitized Solar Cells Based on Superhydrophilic Nanoparticle Coatings. *Nanoscale* **2014**, *6*, 7362−7368.

(6) Wang, S. T.; Liu, K. S.; Yao, X.; Jiang, L. Bioinspired Surfaces with Superwettability: New Insight on Theory, Design, and Applications. *Chem. Rev.* **2015**, *115*, 8230−8293.

DOI: 10.1021/acsnano.6b03884
ACS Nano 2016, 10, 8591−8602

(7) Lee, D.; Rubner, M. F.; Cohen, R. E. All-Nanoparticle Thin-Film Coatings. *Nano Lett.* **2006**, *6*, 2305−2312.
(8) Cebeci, F. C.; Wu, Z.; Zhai, L.; Cohen, R. E.; Rubner, M. F. Nanoporosity-Driven Superhydrophilicity: A Means to Create Multifunctional Antifogging Coatings. *Langmuir* **2006**, *22*, 2856−2862.
(9) Sun, Z.; Liao, T.; Liu, K.; Jiang, L.; Kim, J. H.; Dou, S. X. Fly-Eye Inspired Superhydrophobic Anti-Fogging Inorganic Nanostructures. *Small* **2014**, *10*, 3001−3006.
(10) Chen, Y.; Zhang, Y. B.; Shi, L.; Li, J.; Xin, Y.; Yang, T. T.; Guo, Z. G. Transparent Superhydrophobic/ Superhydrophilic Coatings for Self-Cleaning and Anti-Fogging. *Appl. Phys. Lett.* **2012**, *101*, 033701.
(11) Zhang, X. J.; He, J. H. Antifogging Antireflective Thin Films: Does the Antifogging Layer Have to Be the Outmost Layer? *Chem. Commun.* **2015**, *51*, 12661−12664.
(12) Feng, L.; Li, S. H.; Li, Y. S.; Li, H. J.; Zhang, L. J.; Zhai, J.; Song, Y. L.; Liu, B. Q.; Jiang, L.; Zhu, D. B. Super-Hydrophobic Surfaces: From Natural to Artificial. *Adv. Mater.* **2002**, *14*, 1857−1860.
(13) Sanchez, C.; Arribart, H.; Guille, M. M. G. Biomimetism and Bioinspiration as Tools for the Design of Innovative Materials and Systems. *Nat. Mater.* **2005**, *4*, 277−288.
(14) Yan, Y. Y.; Gao, N.; Barthlott, W. Mimicking Natural Superhydrophobic Surfaces and Grasping the Wetting Process: A Review on Recent Progress in Preparing Superhydrophobic Surfaces. *Adv. Colloid Interface Sci.* **2011**, *169*, 80−105.
(15) Bae, W. G.; Kim, H. N.; Kim, D.; Park, S. H.; Jeong, H. E.; Suh, K. Y. 25th Anniversary Article: Scalable Multiscale Patterned Structures Inspired by Nature: The Role of Hierarchy. *Adv. Mater.* **2014**, *26*, 675−700.
(16) Su, B.; Tian, Y.; Jiang, L. Bio-Inspired Interfaces with Super-Wettability: From Materials to Chemistry. *J. Am. Chem. Soc.* **2016**, *138*, 1727−1748.
(17) Barthlott, W.; Neinhuis, C. Purity of the Sacred Lotus, or Escape from Contamination in Biological Surfaces. *Planta* **1997**, *202*, 1−8.
(18) Ju, J.; Bai, H.; Zheng, Y.; Zhao, T.; Fang, R.; Jiang, L. A Multi-Structural and Multi-Functional Integrated Fog Collection System in Cactus. *Nat. Commun.* **2012**, *3*, 1247.
(19) Gao, X. F.; Yan, X.; Yao, X.; Xu, L.; Zhang, K.; Zhang, J. H.; Yang, B.; Jiang, L. The Dry-Style Antifogging Properties of Mosquito Compound Eyes and Artificial Analogues Prepared by Soft Lithography. *Adv. Mater.* **2007**, *19*, 2213−2217.
(20) Chen, H. W.; Zhang, P. F.; Zhang, L. W.; Liu, H. L.; Jiang, Y.; Zhang, D. Y.; Han, Z. W.; Jiang, L. Continuous Directional Water Transport on the Peristome Surface of *Nepenthes alata*. *Nature* **2016**, *532*, 85−89.
(21) Shi, F.; Niu, J.; Liu, J.; Liu, F.; Wang, Z.; Feng, X. Q.; Zhang, X. Towards Understanding Why a Superhydrophobic Coating Is Needed by Water Striders. *Adv. Mater.* **2007**, *19*, 2257−2261.
(22) Katifori, E.; Alben, S.; Cerda, E.; Nelson, D. R.; Dumais, J. Foldable Structures and the Natural Design of Pollen Grains. *Proc. Natl. Acad. Sci. U. S. A.* **2010**, *107*, 7635−7639.
(23) Kim, J. H.; Moon, J. H.; Lee, S. Y.; Park, J. Biologically Inspired Humidity Sensor Based on Three-Dimensional Photonic Crystals. *Appl. Phys. Lett.* **2010**, *97*, 103701.
(24) Peng, W. H.; Zhu, S. M.; Zhang, W.; Yang, Q. Q.; Zhang, D.; Chen, Z. X. Spectral Selectivity of 3D Magnetophotonic Crystal Film Fabricated from Single Butterfly Wing Scales. *Nanoscale* **2014**, *6*, 6133−6140.
(25) Xu, Z.; Yu, K.; Li, B.; Huang, R.; Wu, P.; Mao, H. B.; Liao, N.; Zhu, Z. Q. Optical Properties of SiO_2 and ZnO Nanostructured Replicas of Butterfly Wing Scales. *Nano Res.* **2011**, *4*, 737−745.
(26) Potyrailo, R. A.; Ghiradella, H.; Vertiatchikh, A.; Dovidenko, K.; Cournoyer, J. R.; Olson, E. *Morpho* Butterfly Wing Scales Demonstrate Highly Selective Vapour Response. *Nat. Photonics* **2007**, *1*, 123−128.
(27) Han, Z. W.; Niu, S. C.; Shang, C. H.; Liu, Z. N.; Ren, L. Q. Light Trapping Structures in Wing Scales of Butterfly *Trogonoptera brookiana*. *Nanoscale* **2012**, *4*, 2879−2883.
(28) Zhang, W.; Zhang, D.; Fan, T. X.; Gu, J. J.; Ding, J.; Wang, H.; Guo, Q. X.; Ogawa, H. Novel Photoanode Structure Templated from Butterfly Wing Scales. *Chem. Mater.* **2009**, *21*, 33−40.
(29) Wiederhecker, G. S.; Chen, L.; Gondarenko, A.; Lipson, M. Controlling Photonic Structures Using Optical Forces. *Nature* **2009**, *462*, 633−636.
(30) Han, Z. W.; Mu, Z. Z.; Li, B.; Niu, S. C.; Zhang, J. Q.; Ren, L. Q. A High-Transmission, Multiple Antireflective Surface Inspired from Bilayer 3D Ultrafine Hierarchical Structures in Butterfly Wing Scales. *Small* **2016**, *12*, 713−720.
(31) Han, Z. W.; Mu, Z. Z.; Yin, W.; Li, W.; Niu, S. C.; Zhang, J. Q.; Ren, L. Q. Biomimetic Multifunctional Surfaces Inspired from Animals. *Adv. Colloid Interface Sci.* **2016**, *234*, 27−50.
(32) Gavartin, E.; Braive, R.; Sagnes, I.; Arcizet, O.; Beveratos, A.; Kippenberg, T. J.; Robert-Philip, I. Optomechanical Coupling in a Two-Dimensional Photonic Crystal Defect Cavity. *Phys. Rev. Lett.* **2011**, *106*, 203902.
(33) Sambles, J. R. Biophotonics: Blue Butterflies Feel the Heat. *Nat. Photonics* **2012**, *6*, 141−142.
(34) Liu, C. C.; Ju, J.; Zheng, Y. M.; Jiang, L. Asymmetric Ratchet Effect for Directional Transport of Fog Drops on Static and Dynamic Butterfly Wings. *ACS Nano* **2014**, *8*, 1321−1329.
(35) Berthier, S.; Charron, E.; Da Silva, A. Determination of the Cuticle Index of the Scales of the Iridescent Butterfly *Morpho Menelaus*. *Opt. Commun.* **2003**, *228*, 349−356.
(36) Chung, K.; Yu, S.; Heo, C. J.; Shim, J. W.; Yang, S. M.; Han, M. G.; Lee, H. S.; Jin, Y.; Lee, S. Y.; Park, N.; Shin, J. H. Flexible, Angle-Independent, Structural Color Reflectors Inspired by *Morpho* Butterfly Wings. *Adv. Mater.* **2012**, *24*, 2375−2379.
(37) Vukusic, P.; Sambles, J. R. Photonic Structures in Biology. *Nature* **2003**, *424*, 852−855.
(38) Seago, A. E.; Brady, P.; Vigneron, J. P.; Schultz, T. D. Gold Bugs and Beyond: A Review of Iridescence and Structural Colour Mechanisms in Beetles (*Coleoptera*). *J. R. Soc., Interface* **2009**, *6*, S165−S184.
(39) Chung, K.; Shin, J. H. Range and Stability of Structural Colors Generated by *Morpho*-Inspired Color Reflectors. *J. Opt. Soc. Am. A* **2013**, *30*, 962−968.
(40) Lu, T.; Zhu, S.; Chen, Z.; Wang, W. L.; Zhang, W.; Zhang, D. Hierarchically Photonic Structured Stimuli-Responsive Materials as High-Performance Colorimetric Sensors. *Nanoscale* **2016**, *8*, 10316−10322.
(41) Zhang, S. C.; Chen, Y. F.; Lu, B. R.; Liu, J. P.; Shao, J. H.; Xu, C. Lithographically Generated 3D Lamella Layers and Its Structural Color. *Nanoscale* **2016**, *8*, 9118−9127.
(42) Dou, X. Q.; Zhang, D.; Feng, C.; Jiang, L. Bioinspired Hierarchical Surface Structures with Tunable Wettability for Regulating Bacteria Adhesion. *ACS Nano* **2015**, *9*, 10664−10672.
(43) Zheng, Y. M.; Gao, X. F.; Jiang, L. Directional Adhesion of Superhydrophobic Butterfly Wings. *Soft Matter* **2007**, *3*, 178−182.
(44) Niu, S. C.; Li, B.; Mu, Z. Z.; Yang, M.; Zhang, J. Q.; Han, Z. W.; Ren, L. Q. Excellent Structure-Based Multifunction of *Morpho* Butterfly Wings: A Review. *J. Bionic Eng.* **2015**, *12*, 170−189.
(45) Onda, T.; Shibuichi, S.; Satoh, N.; Tsujii, K. Super-Water-Repellent Fractal Surfaces. *Langmuir* **1996**, *12*, 2125−2127.
(46) Wang, R.; Hashimoto, K.; Fujishima, A.; Chikuni, M.; Kojima, E.; Kitamura, A.; Shimohigoshi, M.; Watanabe, T. Light-Induced Amphiphilic Surfaces. *Nature* **1997**, *388*, 431−432.
(47) Sun, T. L.; Wang, G. J.; Feng, L.; Liu, B. Q.; Ma, Y. M.; Jiang, L.; Zhu, D. B. Reversible Switching between Superhydrophilicity and Superhydrophobicity. *Angew. Chem., Int. Ed.* **2004**, *43*, 357−360.
(48) Wenzel, R. N. Resistance of Solid Surfaces to Wetting by Water. *Ind. Eng. Chem.* **1936**, *28*, 988−994.
(49) Cassie, A. B. D.; Baxter, S. Wettability of Porous Surfaces. *Trans. Faraday Soc.* **1944**, *40*, 546−551.

DOI: 10.1021/acsnano.6b03884
ACS Nano 2016, 10, 8591−8602